This is the accepted manuscript made available via CHORUS. The article has been published as:

Anomalous descent of intruders in vibrated gas-fluidized granular materials

Oscar J. Punch, Qiang Guo, Maty Gueye, Javad Omidi, Michael W. Jordan, Jagan Mohan Sanghishetty, and Christopher M. Boyce

Phys. Rev. E **111**, L013403 — Published 24 January 2025

DOI: 10.1103/PhysRevE.111.L013403

Anomalous Descent of Intruders in Vibrated Gas-Fluidized Granular Materials

Oscar J. Punch,[1,*] Qiang Guo,[1,2,*] Maty Gueye,[3] Javad Omidi,[1] Michael W. Jordan,[1] Jagan M. Sanghishetty,[1] and Christopher M. Boyce[1,†]

[1] *Department of Chemical Engineering, Columbia University, New York, NY 10027, USA*
[2] *State Key Laboratory of Mesoscience and Engineering, Institute of Process Engineering, Chinese Academy of Sciences, Beijing 100190, China*
[3] *Department of Chemical Engineering, City College of New York, New York, NY 10031, USA*

(Dated: January 16, 2025)

The descent of dense intruder discs through granular material fluidized by vertical gas flow and vibration is investigated experimentally and computationally. Single intruders descend with a velocity which oscillates based on distance above the bottom of the system, which simulations show is due to a spatially dependent void fraction in the granular material changing the effective drag force on the intruder. Two vertically aligned intruders undergo a drafting-kissing-tumbling analog which forms because the bottom intruder decelerates due to particle compaction from the weight of the top intruder.

The descent of a dense object or "intruder" through a fluid or solid particulates is a canonical problem which can probe the rheology and mechanics of a complex material, characterizing the resistance provided by the material to downward motion of the intruder due to gravity [1]. For a conventional fluid, drag force eventually balances with gravity to create a terminal velocity; however, in complex fluids, anomalous behavior has been observed, such as oscillatory [2] and stop-go [3] descent, due to viscoelastic and discontinuous-shear-thickening phenomena, respectively.

Dry granular materials exhibit properties which blend the lines between fluids and solids [4], and exhibit a resistance force on intruders which scales linearly with penetration depth, after an initial resistive force due to impact velocity [5]. If the density ratio between intruders and granular particles is above 70, an intruder can descend infinitely through grains reaching a terminal velocity [6], yet below this value, the intruder is eventually stopped due to particles becoming jammed below the intruder [7]. Vertical vibration or gas flow can overcome gravitational force on grains to "fluidize" the particles into a fluid-like state, as often used industrially to convey or mix particles [8, 9]. Vertical vibration of grains can even cause some intruders to rise in a process known as the Brazil nut effect [10]. Intruders with a density ratio greater than 1.2 typically descend infinitely through gas-fluidized grains after quickly reaching a terminal velocity. An anomalous phenomenon of a less dense intruder descending further through grains than a denser intruder has been observed in grains subject to gas flow just below that needed to fluidize the grains, due to the formation of bubbles surrounding the intruder [11, 12].

Vibrated gas-fluidized beds can exhibit favorable behavior for industrial processes, and these systems have been demonstrated to create lattice-structured bubbling dynamics due to local, transient transitions between fluid-like and solid-like behavior in grains [13]. Further, a state has been observed in vibrated gas-fluidized grains in which particles fluidize without the formation of gas bubbles in which particles have exhibited analogs to Rayleigh-Benard convection [14], Faraday waves [15] and Rayleigh-Taylor instabilities [16].

In this Letter, we investigate the descent of disc-shaped intruders through a vibrated gas-fluidized bed in the bubble-free fluidization state, demonstrating a fluctuating descent velocity. Simulations reveal that velocity fluctuations occur due to a varying gas void fraction surrounding intruders in turn generating a fluctuating drag force on the intruder. This void fraction distribution depends on the vertical position of the intruder in the system, but is independent of the starting position. When two intruders descend, the upper intruder catches up to the lower intruder, and the doublet then rotates to descend side-by-side in a phenomenon analogous to drafting-kissing-tumbling [17]. However, rather than the upper intruder accelerating, the lower intruder decelerates and nearly stops during the catch up stage, which simulations demonstrate occurs due to particle compaction around the bottom intruder due to the added weight of the top intruder. These insights shed light on the complex dynamics and rheology of vibrated gas-fluidized grains, and the subsequent effects on intruders with a wide range of potential for manipulation in industry, construction and agriculture.

Experimental—A vibrated gas-fluidized bed was formed by continuously flowing air evenly through a porous metal distributor into a pseudo-2D box (500 mm height × 200 mm width × 8.8 mm depth) of granular particles and placing the system on an electrodynamic shaker (Fig. 1). Disc-shaped steel intruders of density 7800 kg/m^3, diameter 30 mm and thickness 4.8 mm were placed at desired initial positions in the system using a magnet while following a fluidization and intruder move-

* These authors contributed equally
† cmb2302@columbia.edu

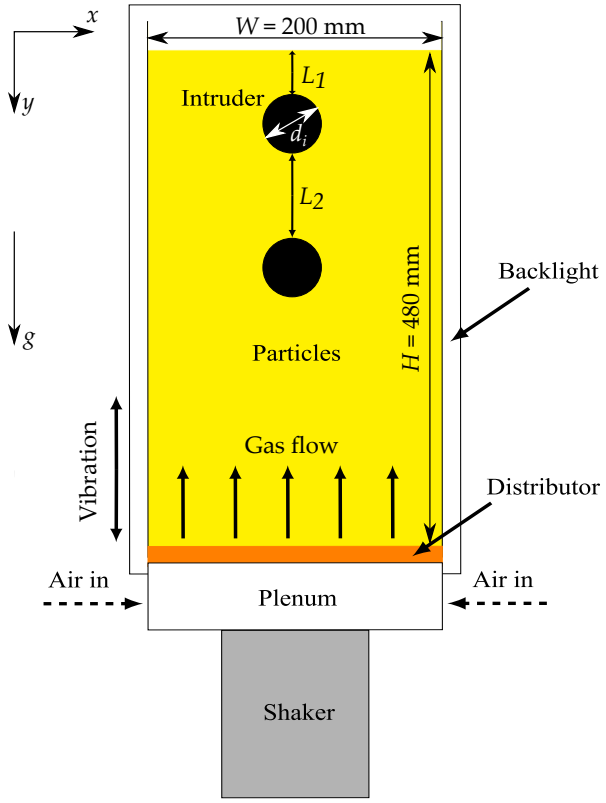


FIG. 1. Schematic of the experimental setup.

ment protocol to avoid effects of initial particle packing and the startup of gas flow and vibration on the descent of the intruders (further details in Supplemental Information [18]). The granular particles consist of monodisperse spherical glass beads with diameter 0.90 mm and density 2500 kg/m^3, which were filled to a height H in the system. No crystallization was observed during experiments. The superficial gas velocity (U) was operated below the minimum gas velocity needed to fluidize the particles (U_{mf}), achieving $U/U_{mf} = 0.95$. The system is vibrated vertically using a sinusoidal vibration profile with a frequency of 20 Hz and an amplitude of 0.75 mm, corresponding to a peak acceleration of 0.6 g, where g is gravity. Optical imaging and digital image analysis were used to determine the position and velocity of the intruder over time. Experiments are performed in triplicate and the averaged results are presented. Intruders remained stationary if gas flow or vibration alone were used for the conditions considered here.

Simulations—Computational fluid dynamics–discrete element method (CFD–DEM) [19, 20] simulations were conducted in which a CFD grid size larger than particles was used to model gas flow. DEM was used to track the motion of particles based on Newtonian mechanics with springs, dashpots, and friction used to model particle-particle and particle-wall contact forces [19]. Intruders were modeled as a set of granular particles adhered together. Two way gas-solid coupling was achieved through buoyancy and a drag law [21]. The system size as well as the particle and intruder size and density were identical to those in experiments. Vibration was modeled by oscillating the gravitational force on the particles to model the system in the moving reference frame of the vibrated bed. Further details are given in the Supplemental Information.

Terminal velocity model—The expected terminal velocity of a single intruder was estimated based on a force balance, achieving:

$$m_i \frac{dv_i}{dt} = m_i g - m_i g \left(\frac{\rho_{pg}}{\rho_i}\right) - v_i \mu_{pg} \left(4\pi\sigma + \frac{\pi d_i^2}{2z_i}\right), \quad (1)$$

in which the first term represents gravitational force, the second term buoyant force and the third term drag force with contribution from around the disc as well as between the disc and the front and back walls of the system. v_i is the intruder velocity, m_i is the mass of the intruder, ρ_{pg} is the density of the particle-gas mixture, ρ_i is the density of the intruder, d_i is the diameter of the intruder and z_i is the separation distance between the intruder face and the front wall (which is also equal to the distance between the opposite intruder face and the back wall). μ_{pg} is the effective viscosity of the particle-gas mixture which is approximated to be 1 Pa s due to prior characterization of gas-fluidized grains [22]. $\sigma = [0.5 - e - ln(Re_i/8)]^{-1}$ [23] in which $Re_i = \rho_{pg} v_i d_i / \mu_{pg}$ is the intruder Reynolds number, which has values $0.1 < Re_i < 1$ for this system. Eq. 1 is solved numerically to determine a terminal velocity of 10 mm/s for our single intruder case. We introduce a second equation to empirically correlate intruder descent velocity to local void fraction around the intruder ($\epsilon_{g,i}$) as per,

$$v_i = v_{i,t} \left(\frac{\epsilon_{g,i} - \epsilon_{g,min}}{\overline{\epsilon_g} - \epsilon_{g,min}}\right). \quad (2)$$

Here, $v_{i,t}$ is the terminal velocity for an intruder from Eq. 1, $\overline{\epsilon_g}$ is the temporal mean void fraction around the intruder during descent, and $\epsilon_{g,min}$ is best-fit using regression and found to be $\epsilon_{g,min} = 0.402$ for all cases.

Single intruder descent—A single central intruder descends over time through the grains without significant horizontal displacement or gas bubbles forming (Fig. 2a). The descent velocity quickly accelerates to a peak velocity before decelerating to a velocity close to the estimated terminal velocity. Anomalously, the descent velocity oscillates about this expected terminal velocity with a period of 20 s, far greater than the vibration period (Fig. 2b). When the bed height is decreased (H, Fig. 1), the intruder still descends with an oscillating velocity and after a fast initial descent, the curves for descent velocity

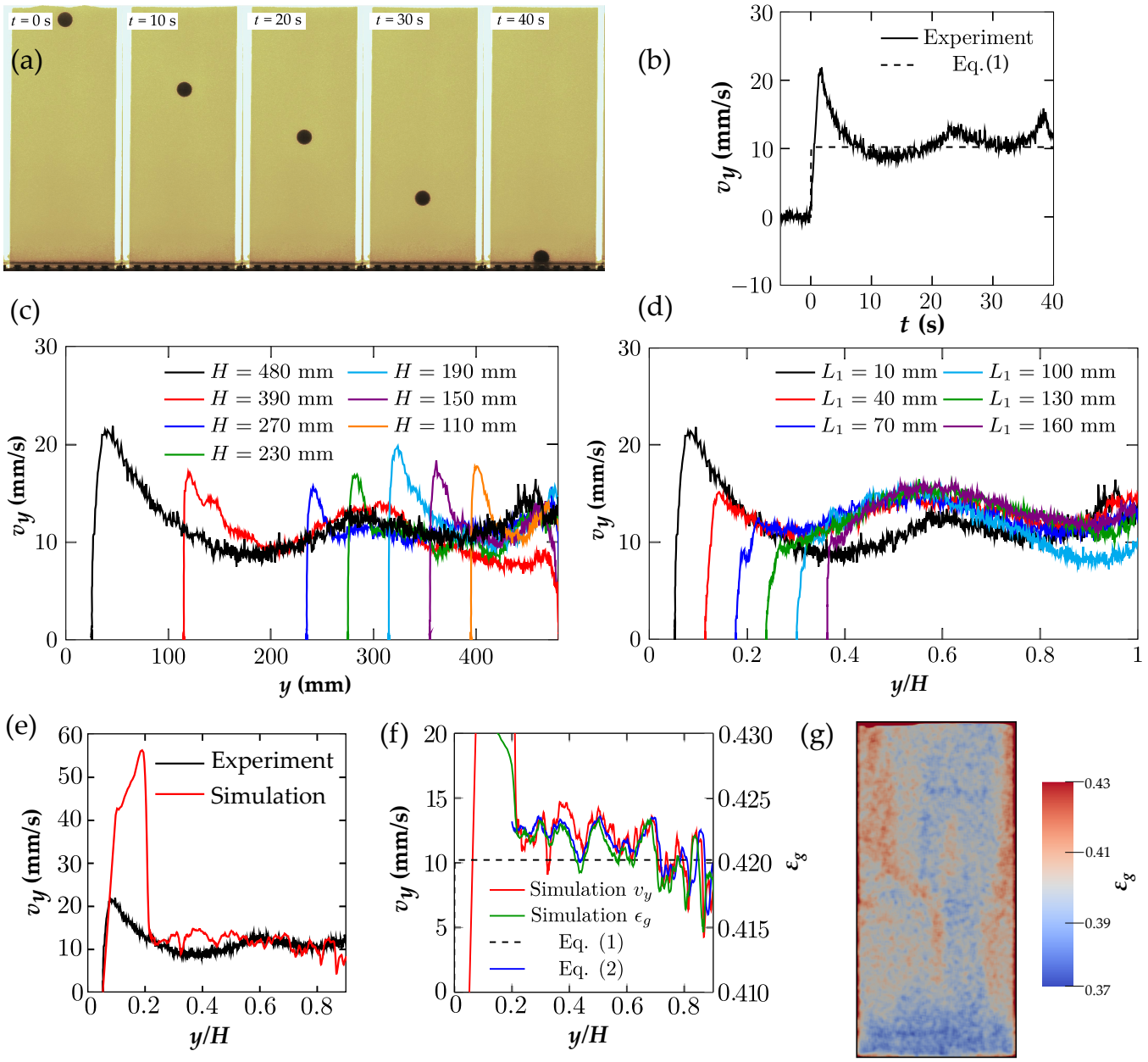


FIG. 2. Descent of a single central intruder: (a) time series of optical images, (b) measured velocity and predicted velocity (Eq. 1), (c) velocity versus vertical position for varying bed height at a constant starting depth ($L_1 = 10$ mm), (d) velocity versus vertical position for different starting positions for a constant bed height ($H = 480$ mm), (e) comparison with CFD-DEM simulations (f) comparison of the local void fraction around the intruder to the simulation intruder descent velocity and the velocity predicted by Eq. 1 and Eq. 2, and (g) CFD-DEM void fraction at $t = 0$ s with no intruder in the system.

collapse based on vertical position above the bottom of the system (Fig. 2c). Furthermore, when the initial distance of the intruder below the bed surface (L, Fig. 1) is increased, and the bed height is constant, the descent velocity collapses with the vertical position of the intruder in the system (Fig. 2d), rather than the velocity history (as would be expected for a non-Newtonian fluid [3]) or the distance displaced (as would be expected for an elastic solid [5]). An oscillatory velocity is also observed when varying the vibration frequency and amplitude (Supplemental Information, Fig. S1). These results suggest that the descent velocity is highly dependent on the distance of the intruder above the bottom of the bed, which contrasts with the concept of hydrostatic pressure varying with distance below the surface of a liquid. CFD-DEM simulations reproduce the experimental results of accelerating early to a peak velocity, followed by decelerating to a velocity of approximately 10 mm/s, about which the ve-

locity fluctuates (Fig. 2e).The higher intruder initial velocity in the simulation is caused by a small wake beneath the intruder which is formed during the vigorous fluidization and resettling initialization process, as the intruder is held constant. Whilst this affects the initial velocity of the intruder, we find that it still quickly approaches the terminal velocity which the velocity then varies around as the intruder descends. The simulation captures the oscillation amplitude, but fails to capture the oscillation characteristic length which may be due to the intruder being porous or that the fluid cells are larger than the particles. The CFD-DEM simulation shows that the gas void fraction surrounding the intruder (taken from a radius of $1.5d_i$ from the centroid of the intruder and excluding the intruder) correlates strongly with the descent velocity (Fig. 2f), demonstrating that with fewer particles surrounding the intruder to provide an effective drag force on the intruder, the intruder descends faster. Further, Fig. 2f reveals that Eq. 2 accurately captures the velocity fluctuations that a Newtonian model (Eq. 1) cannot, highlighting the importance of understanding the linear relationship between local void fraction and intruder velocity. Simulations show that even without an intruder in the system, the complex interaction of gas flow inducing drag and vibration producing sequences of particle contacts creates a spatially varying gas void fraction in the system , for which a snapshot is shown in Fig. 2g. The same spatial variation in void fraction persists over 30 s of simulation. Further, the dependency of descent velocity on distance above the bottom of the system (Fig. 2c,d) indicates that the varying void fraction can be attributed to (i) particle collisions with the bottom plate during vibration and (ii) particle compaction between the intruder and the bottom plate.

Effect of intruder size—When the intruder size is varied, the same trend of oscillating velocity is observed; however, smaller intruders descend faster high in the bed, followed by larger intruders descending faster in the center of the bed, followed by smaller intruders falling faster again low in the bed (Fig. 3a). As such, depending on the amount of time passed, at some points a larger intruder has descended further, while at other points a smaller intruder has descended further (Fig. 3b) (see Supplemental Material Video 1 for a side-by-side descent video comparison). The lead-changing phenomenon, due to a fluctuating velocity, is also observed in numerical simulations (Fig. 3c,d) and the local void fraction around the intruder is well-correlated to the intruder descent velocity (Fig. 3e,f). The intruder descent velocity variations are accurately predicted by Eq. 2. These anomalous descent results differs from what would be expected in a Newtonian fluid at low Re in which larger intruders always descend faster than smaller intruders [24], and further indicated by Eq. 1 failing to predict the approximate terminal velocity. We attribute this behavior to complex effects of intruder size on the surrounding local gas void

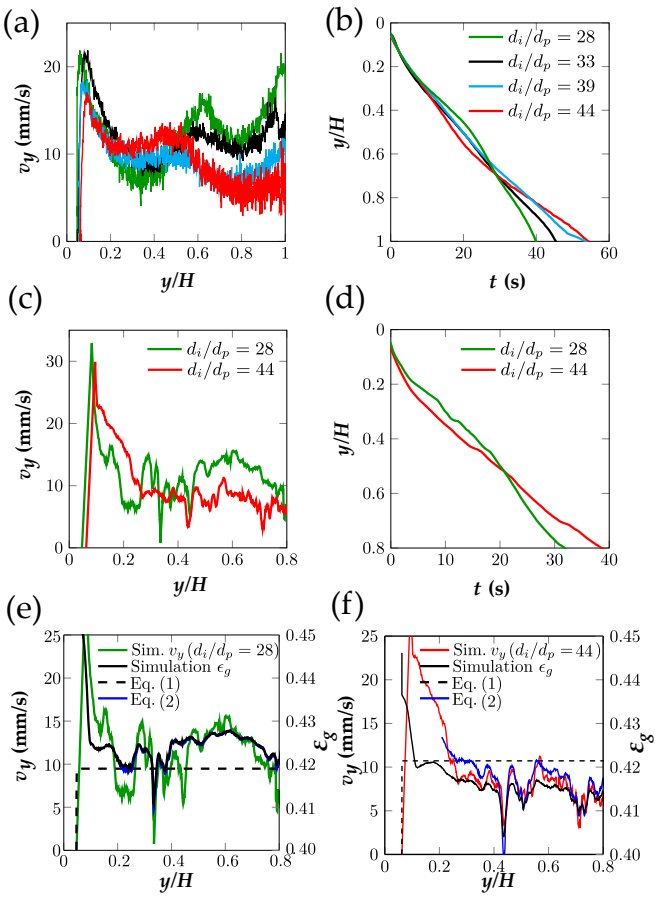


FIG. 3. Effect of intruder diameter on the descent velocity vs. vertical position and the descent position over time for experiments (a,b) and simulations (c,d), respectively. Shown in (e) and (f) is a comparison between the descent velocity to the local void fraction around the intruders and the predicted velocities from Eq. (1) and Eq. (2).

fraction as the intruder descends (Fig. 3e,f) and thus the effective drag force experienced by different sized intruders. In particular, we attribute the slow descent velocity of a larger intruder low in the system to the compression of particles between the bottom of the larger intruder and the bottom of the system under the weight of the larger intruder.

Two vertically aligned intruders—When two intruders are initially aligned vertically (Fig. 4a), the two intruders descend at lower velocities than an isolated intruder (Fig. 4b). The top intruder descends faster than the bottom intruder and catches up to the bottom intruder. The two intruders then rotate about one another while in contact before separating horizontally and then descending side-by-side (Fig. 4a, Supplemental Material Video 2). This phenomenon resembles the drafting-kissing-tumbling phenomenon in conventional fluids with two key differences: (i) the top intruder is not accelerated by wake effects to catch up with the bottom intruder, but

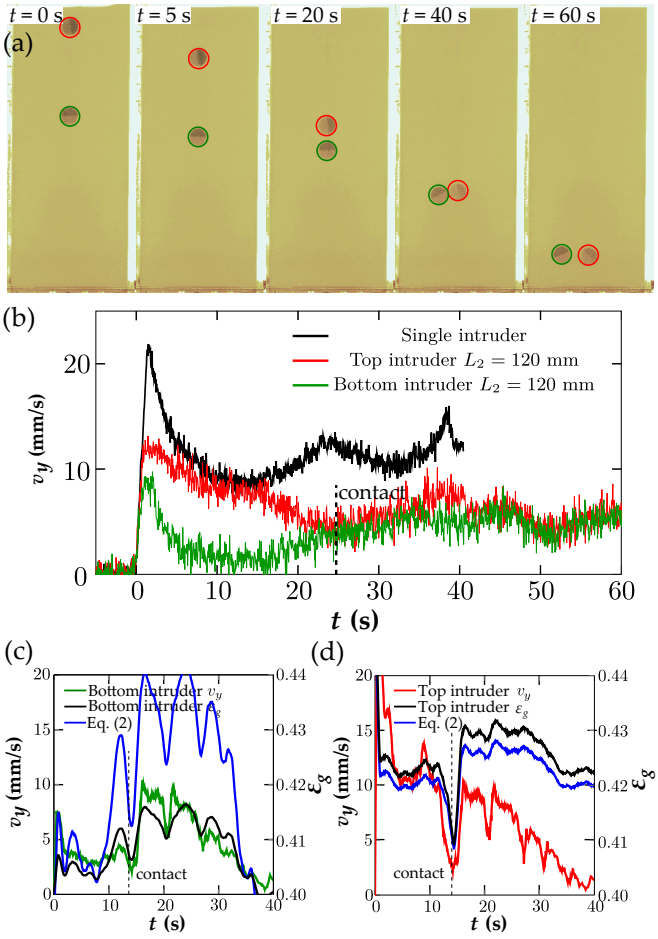


FIG. 4. Descent of two vertically aligned intruders: (a) time series of optical images, (b) descent velocity vs. time as compared to a single intruder, (c,d) CFD-DEM simulation results of descent velocity compared to local void fraction around the intruders and the predicted velocity from Eq. 2 for the (c) bottom and (d) top intruder.

rather the bottom intruder is slowed significantly by the presence of the top intruder, and (ii) the top intruder does not overtake the bottom intruder, instead the two intruders ultimately descend in a stable state side-by-side. The slowing of the bottom intruder allows the top intruder to catch up to the lower intruder even when the intruders are initially separated by distances equaling several intruder diameters (Fig. 4a). CFD-DEM simulations reproduce the experimentally observed phenomena of the top intruder catching up to the bottom intruder before the two tumble as well as the catch up occurring due to the near halting of the bottom intruder. As with the single intruder case, the void fractions surrounding the bottom and top intruders correlate well with the descent velocities of the corresponding intruders (Fig. 4c,d), particularly prior to contact between the intruders. Indeed, Eq. 2 can qualitatively match the simulation prior to collision; yet, after collision different dynamics are observed and Eq. 2 fails to predict the velocity. This difference indicates that further physics than local void fraction must be accounted for when two intruders are descending next to one another. For the bottom intruder, the void fraction is significantly lower than the top intruder or a single intruder, and the descent velocity slows significantly as the void fraction approaches 0.40, nearing the maximum random packing fraction for the grains (Fig. 4c). This slowing phenomenon is attributed to the top intruder compacting grains below it under its weight, thus leading to a lower void fraction surrounding the lower intruder. As such, while a drafting-kissing-tumbling phenomenon is observed, this behavior occurs due to particle compaction effects rather than wake acceleration effects.

Conclusion—Summarizing, we have explored the descent of a dense intruder through grains fluidized by combined vertical gas flow and vibration, which creates a fluid-like state in which transitions to a solid-like state can occur. We have seen that the intruder descends at a velocity which fluctuates with vertical position above the bottom of the system due to different void fractions surrounding the intruder at different positions, which can be accurately predicted using a correlation between local void fraction around the intruder, theoretical minimum void fraction, and terminal velocity. The different void fraction surrounding the intruders at different positions are attributed to complex effects of gas flow and vibration on particle dynamics. This variable void fraction also leads to an anomaly of larger intruders descending faster in certain regions while smaller intruders descend faster in other regions of the system. When two intruders are introduced, a drafting-kissing-tumbling analog is observed, which occurs due to the bottom intruder slowing significantly, rather than the top intruder accelerating. The slowing of the bottom intruder occurs due to particle compaction by the top intruder, causing the particles surrounding the bottom intruder to transition into a solid-like state. Overall, these results demonstrate the complex and locally varying rheology of vibrated gas-fluidized grains, providing potential opportunities to manipulate this behavior with gas flow and vibration conditions to in turn manipulate the motion of larger objects in granular processes.

This work was financially supported by Office of Naval Research grant N00014-23-1-2041 and National Science Foundation grants 2144763 and 2150296 and Sloan Foundation grant G-2021-17054. The authors would like to thank Christopher J. Durning for stimulating discussions.

[1] L. Rayleigh, LIII. On the resistance of fluids, London Edinburgh Philos. Mag. & J. Sci. **2**, 430–441 (1876).
[2] M. T. Arigo, D. Rajagopalan, N. Shapley, and G. H. McKinley, The sedimentation of a sphere through an elastic fluid. Part 1. Steady motion, Journal of Non-

Newtonian Fluid Mechanics **60**, 225–257 (1995).
[3] S. von Kann, J. H. Snoeijer, and D. van der Meer, Velocity oscillations and stop-go cycles: The trajectory of an object settling in a cornstarch suspension, Phys. Rev. E **87**, 042301 (2013).
[4] B. Andreotti, Y. Forterre, and O. Pouliquen, *Granular Media: Between Fluid and Solid*, (Cambridge University Press, 2013).
[5] L. K. Roth, E. Han, and H. M. Jaeger, Intrusion into Granular Media Beyond the Quasistatic Regime, Phys. Rev. Lett. **126**, 218001 (2021).
[6] F. Pacheco-Vazquez, G. A. Caballero-Robledo, J. M. Solano-Altamirano, E. Altshuler, A. J. Batista-Leyva, and J. C. Ruiz-Suarez, Infinite Penetration of a Projectile into a Granular Medium, Phys. Rev. Lett. **106**, 218001 (2011).
[7] H. Zheng, D. Wang, D. Z. Chen, M. Wang, and R. P. Behringer, Intruder friction effects on granular impact dynamics, Phys. Rev. E **98**, 032904 (2018).
[8] J. F. Davidson, *Fluidised Particles*, (Cambridge University Press, 1963).
[9] A. Gnoli, L. de Arcangelis, F. Giacco, E. Lippiello, M. P. Ciamarra, A. Puglisi, and A. Sarracino, Controlled Viscosity in Dense Granular Materials, Phys. Rev. Lett. **120**, 138001 (2018).
[10] A. Rosato, K. J. Strandburg, F. Prinz, and R. H. Swendsen, Why the Brazil nuts are on top: Size segregation of particulate matter by shaking, Phys. Rev. Lett. **58**, 1038–1040 (1987).
[11] J. Oshitani, T. Sasaki, T. Tsuji, and K. Higashida, and D. Y. C. Chan, Anomalous Sinking of Spheres due to Local Fluidization of Apparently Fixed Powder Beds, Phys. Rev. Lett. **116**, 068001 (2016).
[12] T. Tsuji, A. Penn, T. Hattori, K. P. Pruessmann, C. R. Muller, J. Oshitani, K. Washino, and T. Tanaka, Mechanism of anomalous sinking of an intruder in a granular packing close to incipient fluidization, Phys. Rev. Fluids **6**, 064305 (2021).
[13] Q. Guo, Y. Zhang, A. Padash, K. Xi, T. M. Kovar, and C. M. Boyce, Dynamically structured bubbling in vibrated gas-fluidized granular materials, Proc. Nat. Acad. Sci. U.S.A. **118**, e2108647118 (2021).
[14] Q. Guo, Y. Zhang, T. M. Kovar, K. Xi, and C. M. Boyce, A Rayleigh–Bénard convection instability analog in vibrated gas-fluidized granular particles, Soft Matter **18**, 3323–3327 (2022).
[15] Q. Guo, W. Da, R. Wu, Y. Zhang, J. Wei, and C. M. Boyce, Faraday wave instability analog in vibrated gas-fluidized granular particles, Phys. Rev. E **107**, 034603 (2023).
[16] C. P. McLaren, T. M. Kovar, A. Penn, C. R. Müller, and C. M. Boyce, Gravitational instabilities in binary granular materials, Proc. Nat. Acad. Sci. U.S.A. **116**, 9263–9268 (2019).
[17] A. F. Fortes, D. D. Joseph, T. S. Lundgren, Nonlinear mechanics of fluidization of beds of spherical particles, J. Fluid Mech. **177**, 467–483 (1987).
[18] See Supplemental Material at, which includes Refs. [19], for the supplemental videos, further details describing the experimental setup and numerical simulations, and the effect of varying frequency and vibration strength on the descent of a single intruder.
[19] M. Syamlal, W. Rogers, and T. J. O'Brien, MFiX documentation theory guide (1993).
[20] P. A. Cundall and O. D. Strack, A discrete numerical model for granular assemblies, Geotechnique **29**, 47–65 (1979).
[21] J. Ding and D. Gidaspow, A bubbling fluidization model using kinetic theory of granular flow, AIChE J. **36**, 523–538 (1990).
[22] J. R. Grace, The viscosity of fluidized beds, Can. J. Chem. Eng. **48**, 30–33 (1970).
[23] H. Lamb, XV. On the uniform motion of a sphere through a viscous fluid, London Edinburgh Philos. Mag. & J. Sci. **21**, 112–121 (1911).
[24] S. Dey, S. Z. Ali, and E. Padhi, Terminal fall velocity: the legacy of Stokes from the perspective of fluvial hydraulics, Proc. R. Soc. A **475**, 20190277 (2019).